Analytical Sciences (2022) 38:1433–1440
https://doi.org/10.1007/s44211-022-00178-4

ORIGINAL PAPER

Ultrathin g-C_3N_4 nanosheet–CoOOH nanocomposite for fluorescence imaging of ascorbic acid in living cells

Chang Liu[1] · Xuzi Li[1] · Lijiao Deng[1] · Tao Wu[1] · Guoqiang Zou[2] · Hai Yang[1]

Received: 6 July 2022 / Accepted: 7 August 2022 / Published online: 24 August 2022

Abstract

Ascorbic acid (AA), a critical cellular metabolite involved in many biochemical pathways, is an important antioxidant in human body. Therefore, it is of great significance to monitor AA in living cells. Nowadays, there are various technologies developed for the detection of AA, but few methods could sensitively and selectively detect the intracellular AA. Here, we reported a highly efficient biosensor (g-C_3N_4–CoOOH nanocomposite) based on ultrathin graphitic carbon nitride (g-C_3N_4) nanosheets and CoOOH nanoflakes, for sensitive detection and fluorescence imaging of AA in living cell. The g-C_3N_4 used here as fluorescence donor is a promising bioimaging nanomaterial because of their high fluorescence quantum yield, good biocompatibility and low toxicity. In addition, the CoOOH was used to be perfect fluorescence quencher. Herein, we enabled the CoOOH in situ to form a layer on the surface of g-C_3N_4, resulting in fluorescence quench of the g-C_3N_4. Upon the addition of AA, the CoOOH nanoflakes were reduced to Co^{2+}, and the system gave a "turn on" fluorescence signal. It developed as an efficient sensing platform for AA, and the linear range was from 5 to 50 μM with a 1.6 μM detection limit. This novel biosensor, g-C_3N_4–CoOOH nanocomposite exhibited highly selective response toward AA relative to other biomolecules. Furthermore, this biosensor was used successfully to visualize and monitor AA in living cells. Hopefully, we believe that this biosensor would provide a low-cost and highly sensitive platform for AA detection and bioimaging.

Keywords Ascorbic acid · Graphitic carbon nitride · CoOOH

Introduction

Ascorbic acid (AA) plays as an important micronutrient with many biological processes [1]. In particular, AA participates in various reactions as an enzyme cofactor, such as immune system enhancement, scurvy prevention, collagen synthesis, and enzymatic reactions [2]. Moreover, AA is also a naturally occurring antioxidant, resisting the cells damage from free radical and avoiding cytometaplasia. In previous research, the data showed the level of AA was related to many diseases, such as cardiovascular disease, scurvy, arteriosclerosis, and so on [3, 4]. Therefore, it is critically important to develop effective methods to monitor AA in living cells.

Up until now, some methods have been developed for the detection of AA, including colorimetry [5], electrochemistry [6], and chromatography [7]. However, these methods showed a lack of good biocompatibility, requiring complex separation techniques for extracting AA from cells, limiting the application in live cells. The fluorescence method [8, 9] attracted extensive attention and realized to in situ monitor AA in live cells, due to the advantages of good reproducibility and high sensitivity. Significantly, fluorescence detection of AA has been successfully realized with the help of the organic dye molecule [10, 11]. However, the method based on organic dye molecule suffers the poor photostability and easy photobleaching. On the basis of the redox reaction between CoOOH and AA, Tan's group reported near-infrared (NIR) graphene quantum dots (GQD) as a two-photon (TP) nanoprobe for detecting and bioimaging endogenous AA in live cells [12]. So, it is of great significance to develop

✉ Chang Liu
liuchang202205@163.com

✉ Guoqiang Zou
gq-zou@csu.edu.cn

✉ Hai Yang
yanghai1001@163.com

[1] School of Chemistry and Chemical Engineering, Hunan Institute of Engineering, Xiangtan 411104, Hunan, China

[2] College of Chemistry and Chemical Engineering, Central South University, Changsha 410083, Hunan, China

some efficient fluorescence nanoprobes based on redox reaction between CoOOH and AA, for the determination of AA.

Recently, fluorescent graphitic carbon nitride (g-C_3N_4), as a promising candidate to expand carbon materials application, has attracted tremendous attention due to the high fluorescence quantum yield, robust chemical inertness, low toxicity, and good biocompatibility [13]. Therefore, taking the advantage of high fluorescence quantum yield and excellent bleaching resistance, the g-C_3N_4 became an ideal material for constructing a robust platform for biosensors [14–20]. Moreover, the g-C_3N_4 can be internalized efficiently into live cells by endocytosis [21]. Recently, more and more researchers pay attention to the metal-free g-C_3N_4 for bioimaging and biomedical applications. Due to the fact that the g-C_3N_4 possesses excellent adsorption capacity for single-stranded DNA, and the N-containing structure of the g-C_3N_4 can coordinate with protons or metal ions, nanocomposites based on the g-C_3N_4 have been explored to effectively detect the various important biomolecules in live cells [22–26]. However, up to now, the nanomaterials based on g-C_3N_4 were not applied to detect the AA in live cells.

In a sensing platform, the g-C_3N_4 could be fluorophore (donor), which transferred its energy to quencher (acceptor) within the distance of 10 nm. CoOOH nanosheets, a 2D layered nanomaterial possessing excellent optical, electronic and thermal properties, are considered as emerging quencher candidates [27, 28]. For example, You et al. used aptamer-modified g-CNQDs and CoOOH nanosheets as donor–acceptor pair, taking energy transfer-based fluorescence aptasensor to detect Ochratoxin A [29]. Hu et al. applied MoS_2 QDs as the fluorescence elements and CoOOH nanoflakes as scattered light units to measured AA [30].

In this work, we designed a novel nanocomposite for AA image in live cells. The g-C_3N_4–CoOOH nanocomposite was composed of g-C_3N_4 functionalized with CoOOH, based on that the cobalt ions (Co^{2+}) were effectively adsorbed onto g-C_3N_4 by the interaction between Co^{2+} and the active functional groups (e.g., carboxyl and amino groups) on the surface of the g-C_3N_4 nanosheet, and then the CoOOH could be grown in situ on the surface of g-C_3N_4 nanosheet. The nanocomposites were formed like a sandwich, as the CoOOH was grown on the both sides of the g-C_3N_4 nanosheet. This one-step synthesis method closed the distance between the g-C_3N_4 and the CoOOH nanosheet, constructing the donor–acceptor pair, resulting in that the fluorescence of g-C_3N_4 nanosheet was quenched because of energy transfer from g-C_3N_4 nanosheet to the deposited CoOOH. However, in the presence of AA, the quenched fluorescence could be restored, as AA could reduce CoOOH to Co^{2+}, resulting in the decomposition of the CoOOH from the g-C_3N_4–CoOOH nanocomposite. Remarkably, the nanocomposites showed high sensitivity and selectivity with the low detection limit of 1.6 μM for AA. Besides, taking the advantage of excellent biocompatibility and low toxicity, the nanocomposite was successfully applied for AA image in live cells. This proposed method could develop the application of the 2D nanomaterials of g-C_3N_4.

Experimental section

Materials and instruments

$CuSO_4$, $FeCl_2$, $FeCl_3$, H_2O_2, KCl, $Mg(NO_3)_2$, Na_2CO_3, NaCl, $NiCl_2$, NaOH, NaClO and $ZnCl_2$ were purchased from Beijing Chemical Corp (China). L-Leucine, L-tyrosine, valine, glucose, cysteine (Cys), glutathione (GSH), melamine and AA were obtained from Shanghai Sangon Biotechnology Co., Ltd. (China). $CoCl_2{\cdot}6H_2O$, ascorbate oxidase and *N*-ethylmaleimide were purchased from Sigma-Aldrich, Inc. (USA). The above chemicals were analytical grade and used without further purification. HeLa cells and L02 cells were purchased from the cell bank at Xiangya Hospital (Changsha, China). The ultrapure water used throughout all experiments was purified through a Millipore system (Billerica, MA, USA) with an electric resistance of > 18.3 MΩ.

The fluorescence spectra were measured with a FL-7000 spectrometer (Hitachi, Japan). UV–Vis spectra were performed on a UV5800 spectrophotometer (Shimadzu, Japan). The transmission electron microscopy (TEM) images were obtained on a field-emission high-resolution 2100F TEM (JEOL, Japan). Fourier transform infrared (FTIR) spectra were observed by a Nicolet Nexus 670 FTIR instrument (Nicolet Instrument, USA). The atomic force microscopy (AFM) images were recorded by a Bruker Bioscope system (Bruker, USA). Fluorescence images were carried out using an oil dipping objective (100×, NA 1.2) on Nikon confocal laser scanning fluorescence microscope (Nikon, Japan).

Preparation of ultrathin g-C_3N_4 nanosheets

The g-C_3N_4 nanosheet was prepared according to previous report [19]. In short, bulk g-C_3N_4 was fabricated from the pyrolysis of melamine, through heating 10.0 g ground melamine powders for 3 h to 550 °C with a heating rate of 3 °C·min^{-1}, maintaining it at this temperature for 4 h under air condition. Then, to obtain the highly water-dispersible g-C_3N_4 nanosheet, the bulk g-C_3N_4 was chemically oxidized with nitric acid and underwent a liquid exfoliating process. Briefly, 100 mg finely ground bulk g-C_3N_4 powder was put into 100 mL of 5 M HNO_3 and refluxed for 24 h. After natural cooling to room temperature, the refluxed product was centrifuged at 10,000 rpm for 30 min and washed with water until neutral. The remaining sediment was dispersed in 10 mL ultrapure water and then given ultrasonic treatment for 16 h. Finally, the suspension was centrifuged at

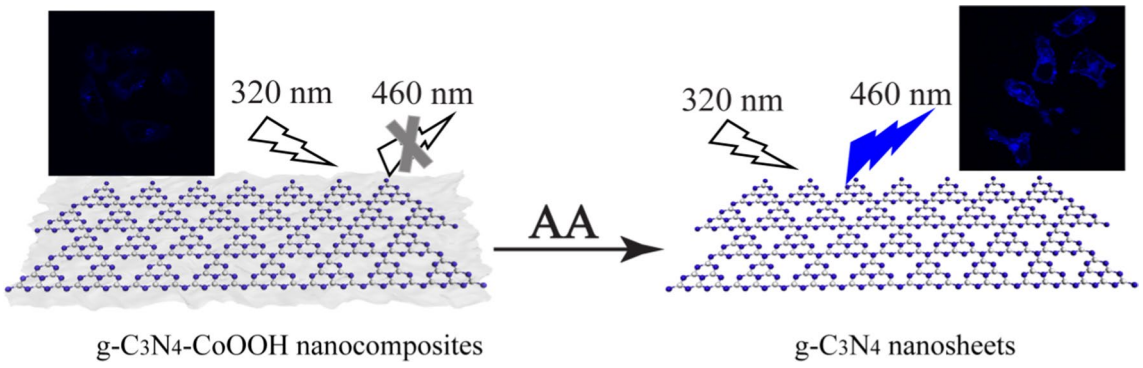

Scheme 1 Schematic illustration of the sensing strategy based on the g-C_3N_4–CoOOH nanocomposite for AA detection

8000 rpm for 15 min to remove the residual unexfoliated g-C_3N_4 nanosheet.

Preparation of g-C_3N_4–CoOOH nanocomposite

In a typical reaction, remaining sediment was redispersed in water for further use. Then, 100 µL of the g-C_3N_4 nanosheet solution (1.0 mg·mL^{-1}) was added to the $CoCl_2$ solution (10 mM, 300 µL) and incubated for 1 h. Second, 100 µL of NaClO (0.2 M) and 100 µL of NaOH (0.8 M) were added to the above solution and sonicated for 10 min. Then, the CoOOH modified g-C_3N_4 was collected via centrifugation and washed with deionized water three times. Finally, the g-C_3N_4–CoOOH nanocomposite was redispersed in water.

In vitro detection of ascorbic acid

50 µL of freshly prepared g-C_3N_4–CoOOH nanocomposite (4.0 mg·mL^{-1}) was added to 150 µL of 10 mM Tris (pH 7.4) containing varied concentration of AA (0–100 µM). Then, the resulting solution was kept at 37 °C for 15 min. Finally, the solution was subjected to fluorescence measurement with excitation at 320 nm.

Selectivity analysis

The prepared g-C_3N_4–CoOOH nanocomposite was incubated with different analytes for selectivity analysis, including $CuSO_4$, Cys, $FeCl_2$, $FeCl_3$, GSH, H_2O_2, KCl, L-leucine, L-tyrosine, $Mg(NO_3)_2$, Na_2CO_3, NaCl, $NiCl_2$, $ZnCl_2$, $CoCl_2$, and valine.

Cell culture

HeLa cells and L02 cells were cultured in RPMI 1640 medium with 10% fetal bovine serum (FBS), streptomycin (100 units·mL^{-1}), and penicillin (100 units·mL^{-1}). All cells were maintained at 37 °C in a humidified atmosphere containing 5 wt %/vol CO_2.

Cell viability assay

Cells (2×10^3) were seeded on 96-well plate and incubated at 37 °C for 24 h. Then, the cells were washed three times with PBS, and incubated with different concentration of g-C_3N_4–CoOOH nanocomposite (0, 50, 100, 150, 200, and 250 µg·mL^{-1}, respectively) for 2.5 h, 5.0 h and 7.5 h, respectively. The cells were washed three times with PBS. And the cells were incubated with the 100 µL culture medium containing 20 µL of MTS reagent for another 1 h. Finally, the cell viability was acquired on an ELx800™ microplate reader to assess the cell viability.

Confocal fluorescence imaging of AA

HeLa cells were cultivated in 35 mm confocal dish for 24 h. After that, the cells were washed with PBS, and then incubated with the RPMI 1640 medium containing 100 µg·mL^{-1} nanocomposite at 37 °C in 5% CO_2 for 2.5 h. Then, the cells were washed with PBS, and incubated with 200 µM AA for 2 h. Finally, the cells were washed with PBS before imaging by using an oil dipping objective (100×, 1.25 NA) on a Nikon confocal laser scanning fluorescence microscope.

Results and discussion

Design principle of g-C_3N_4–CoOOH nanocomposite

The strategy of g-C_3N_4–CoOOH nanocomposite for AA image is presented in Scheme 1. We constructed g-C_3N_4–CoOOH nanocomposite by one-step synthesis method, taking the g-C_3N_4 as the fluorescence donor and the CoOOH as the fluorescence acceptor. In practice, the fluorescence of the g-C_3N_4 at 460 nm was quenched by CoOOH

nanosheets, due to the close distance between the g-C_3N_4 and CoOOH nanosheets triggering the energy transfer reaction. With the addition of AA, depending on the reducibility of AA, the AA could reduce the CoOOH to be Co^{2+}. Meanwhile, CoOOH nanosheets were destroyed, with the recovery of the g-C_3N_4 fluorescence. Therefore, the novel strategy provided a sensitive and selective platform for the AA detection, and AA image in live cells.

Characterization of g-C_3N_4–CoOOH nanocomposite

To reveal the characteristic of the nanocomposite, the TEM, XPS, AFM, FTIR were recorded. The TEM image of g-C_3N_4 (Fig. 1A) and g-C_3N_4–CoOOH nanocomposite (Fig. 1B) showed the typical layered platelet-like morphology. And the TEM image of g-C_3N_4 and g-C_3N_4–CoOOH nanocomposite indicated that CoOOH successfully deposited on the g-C_3N_4 nanosheets, by comparing the change of morphology.

To further investigate morphological changes of the g-C_3N_4–CoOOH nanocomposite, AFM was performed. Corresponding AFM characterization of g-C_3N_4 and g-C_3N_4–CoOOH nanocomposite verified the above TEM results. The sonication treated g-C_3N_4 nanosheets presented a topological height of ~ 3.5 nm, which was typical of the single- or double-layered sheets of g-C_3N_4 (Fig. 1C, D). After the deposition of the CoOOH on the surface of the g-C_3N_4 nanosheets, the topological height

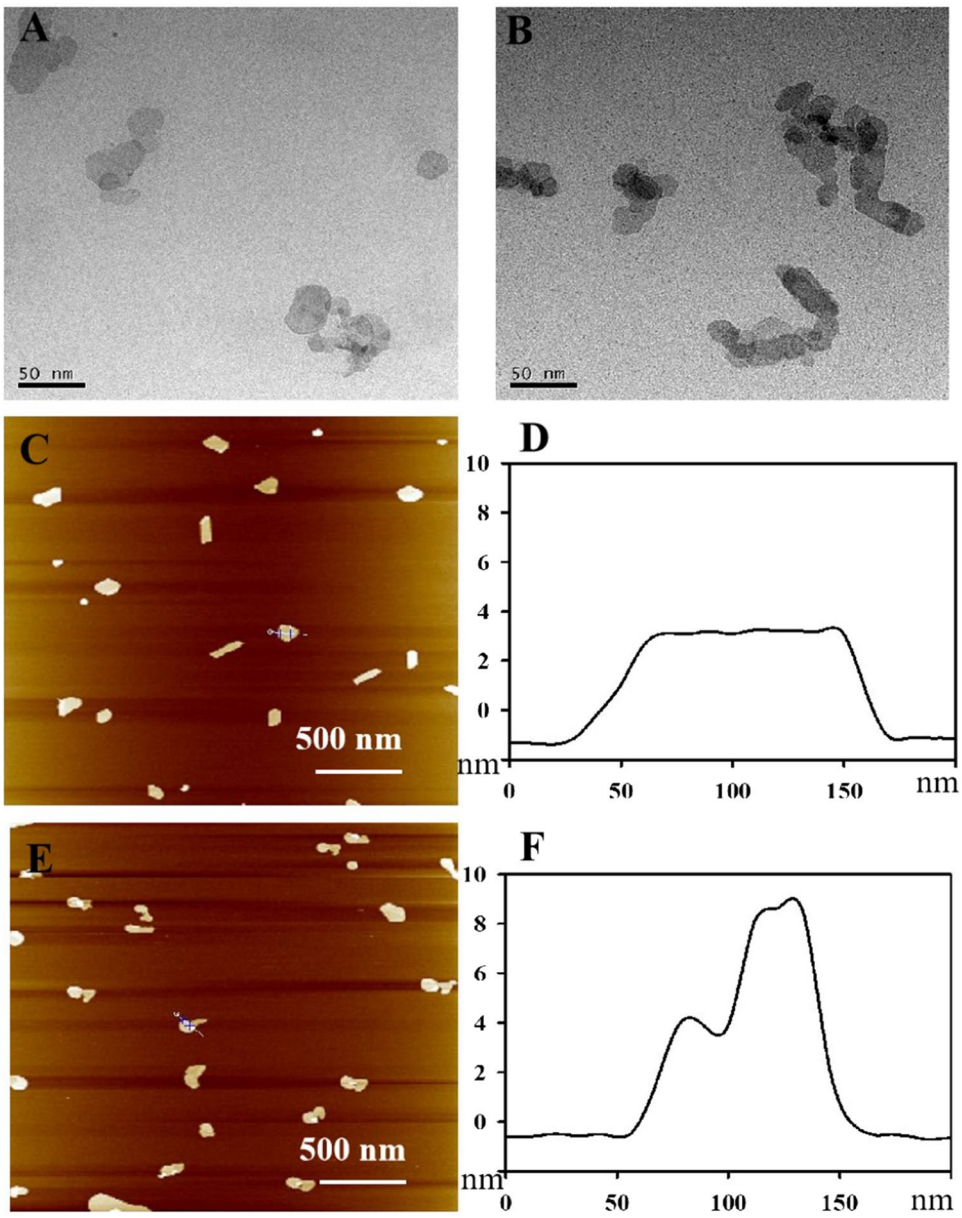

Fig. 1 TEM images of g-C_3N_4 (**A**) and g-C_3N_4–CoOOH nanocomposite (**B**). AFM images (left) and height profiles (right) of g-C_3N_4 (**C,D**) and g-C_3N_4–CoOOH nanocomposite (**E,F**)

of nanocomposites ranged from 3.5 to 9 nm, proving that the CoOOH effectively deposited on the g-C_3N_4 nanosheets (Fig. 1E, F).

As shown in Fig. 2A, the XPS characterizations of g-C_3N_4 showed the existence of C and N. The binding energy peaks representing C 1 s, N 1 s and O 1 s exhibited at 288.12, 399.11, and 533.75 eV in the full range of XPS analysis, respectively. The C 1 s spectrum showed two peaks at 284.82 eV (C–C) and 288.22 eV (N–C=N), respectively (Fig. 2B). In Fig. 2C, the N 1 s spectrum could be split into three peaks, C=N–O at 398.98 eV, N–$(C)_3$ at 400.04 eV and C–N–H at 401.33 eV [31]. Furthermore, we investigated the XPS analysis of g-C_3N_4–CoOOH nanocomposite. As shown in Fig. 2D, E, two peaks at 797.28 eV (Co $2p_{1/2}$) and 782.01 eV (Co $2p_{3/2}$) implied that the CoOOH nanoflakes were deposited on the g-C_3N_4, and the cobalt of the CoOOH nanoflakes was Co (III) oxidation state.

Then FTIR spectra (Fig. S1) were applied to reveal the surface chemistry of the g-C_3N_4 (black) and g-C_3N_4–CoOOH nanocomposite (red). The characteristic absorption peaks from 3000 to 3400 cm^{-1} were attributed to N–H and O–H stretching vibrations. And the peaks at 1100–1700 cm^{-1} were related to C–N vibration and Co–O stretches. Moreover, the sharp peak at 510–650 cm^{-1} ascribed to Co-O^{2-} vibration, demonstrating the CoOOH effectively deposited on the g-C_3N_4 and g-C_3N_4–CoOOH nanocomposite successfully generated. After that, we investigated the UV–Vis absorption spectra of the g-C_3N_4 (black) and g-C_3N_4–CoOOH nanocomposite (red). As shown in Fig. S2, compared with the g-C_3N_4, the UV–Vis absorption peak of g-C_3N_4–CoOOH nanocomposite showed a large red shift from 318 to 388 nm. These above results powerfully indicated that the CoOOH effectively deposited on the g-C_3N_4 nanosheets.

In vitro detection of AA

To ascertain the quenching efficiency of g-C_3N_4 by CoOOH nanosheets, we explored the optical properties of the g-C_3N_4 and CoOOH nanosheets. As shown in Fig. S3, we observed the UV–Vis absorption spectrum of CoOOH nanosheets had a broad absorption band from 300 to 550 nm, which overlapped well with the fluorescence emission (460 nm) of the g-C_3N_4 under the excitation of 320 nm. So, it suggested that the energy transfer from the g-C_3N_4 to the CoOOH was feasible, and the fluorescence of the g-C_3N_4 could be effectively quenched by CoOOH.

Then, to confirm the feasibility of g-C_3N_4–CoOOH nanocomposite for the detection of AA, we explored the fluorescence change of the g-C_3N_4–CoOOH nanocomposite to react with AA. As shown in Fig. S4, the g-C_3N_4–CoOOH nanocomposite showed weak fluorescence signal as the CoOOH had the high fluorescence quenching efficiency of the g-C_3N_4. However, upon the addition of AA into the

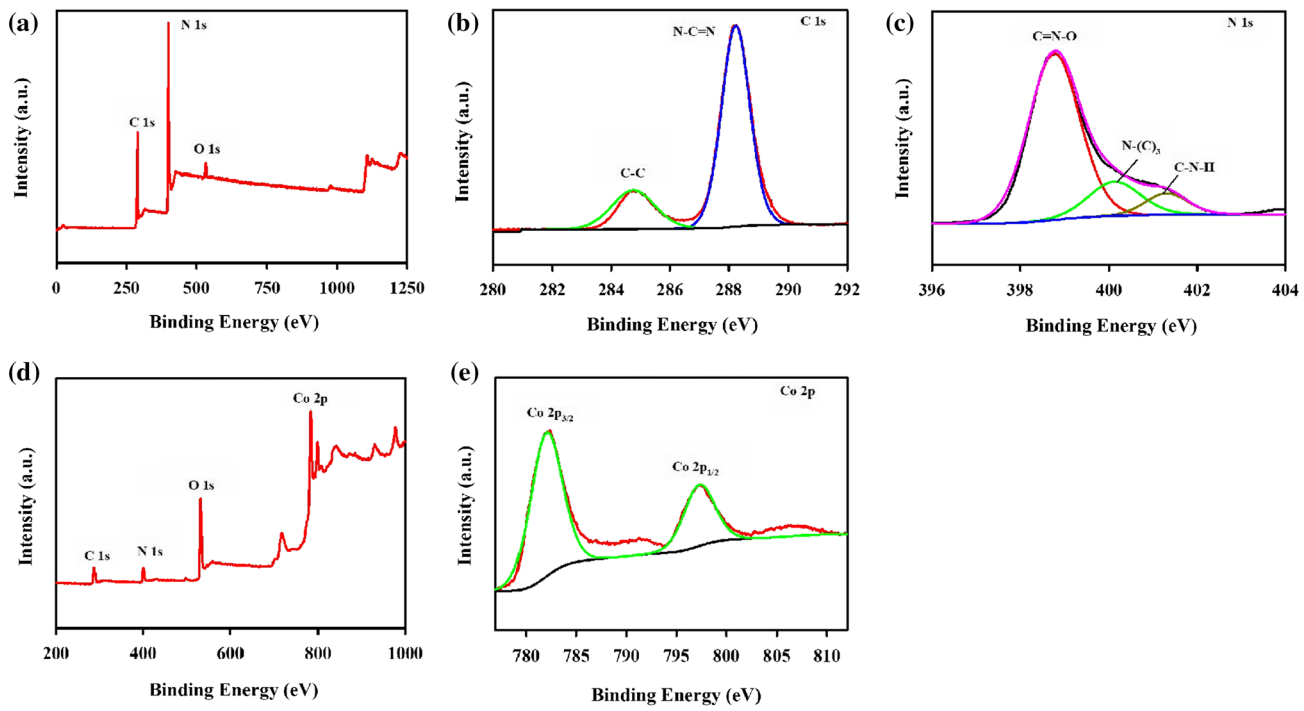

Fig. 2 XPS analysis of **A** g-C_3N_4, **B** C 1 s and **C** N 1 s region of XPS analysis for the g-C_3N_4; XPS analysis of **D** g-C_3N_4–CoOOH nanocomposite and **E** Co 2p region of XPS analysis for the g-C_3N_4–CoOOH nanocomposite

solution containing g-C_3N_4−CoOOH nanocomposite, we observed an obvious fluorescence emission peak at 460 nm with the excitation of 320 nm. The result revealed that the reduction of CoOOH occurred on the g-C_3N_4−CoOOH nanocomposite.

Next, to acquire high performance of g-C_3N_4−CoOOH nanocomposite toward AA, we optimized the experimental conditions including the amount of the Co^{2+}, different buffer, the pH of buffer, and the incubation time. As shown in Fig. S5A, with the increase of the amount of Co^{2+}, the fluorescence of g-C_3N_4 decreased obviously due to the high quenching efficiency of the in situ-synthesized CoOOH on the surface of the g-C_3N_4, and leveled off when the concentration reached 3.0 mM. Then, we examined the different buffer for obtaining the highly sensitive response. The results showed the reaction in the tris buffer could obtain higher fluorescence intensity (Fig. S5B). Subsequently, we investigated the effect of pH on the g-C_3N_4−CoOOH nanocomposite for the assay of AA. The results indicated the assay of the g-C_3N_4−CoOOH nanocomposite toward AA was basically stable under physiological pH conditions from 6.4 to 8.4 (Fig. S5C). Finally, the incubation time was also investigated. The fluorescence intensity exhibited a time-dependent increase, and 8 min was selected for AA reduction reaction (Fig. S5D).

Under the optimized experimental conditions, we investigated the ability of g-C_3N_4−CoOOH nanocomposite for quantitative analysis of AA. As shown in Fig. 3, it showed the fluorescence emission spectra of g-C_3N_4−CoOOH nanocomposite after incubation with varied concentration of AA for 15 min at 37 °C. With the increasing AA concentrations, the fluorescence at 460 nm gradually increased under the excitation of 320 nm. And the intensity of the fluorescence peak at 460 nm exhibited linear correlation to the AA concentration in the range from 5 to 50 μM. The detection limit of AA was estimated to be 1.6 μM (in terms of the rule of 3 times deviation over the blank response). It revealed this nanocomposite could afford a promising platform for highly specific and sensitive detection of AA in live cells. Then, as shown in Table 1, we compared other reported sensors for the detection of AA. It indicated that this sensor was comparable to most of those strategies in limit of detection.

In order to evaluate the specificity of the g-C_3N_4−CoOOH nanocomposite for AA, we investigated some common potentially interfering substances including relevant ions, amino acids and other reducing substances. As shown in Fig. 4, compared with other interfering molecule, the results clearly indicated that the assay had desirable selectivity toward AA, due to the fact that AA could reduce CoOOH to Co^{2+}, and resulted in the fluorescence recovery of the g-C_3N_4−CoOOH nanocomposites. It provided potential platform for the application to detect intracellular AA.

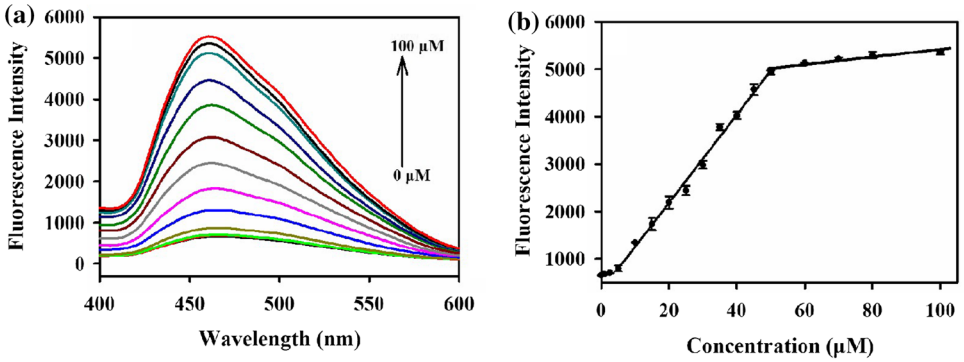

Fig. 3 **A** Fluorescence spectral responses to varying concentrations of AA and **B** correlation curve of fluorescence intensities (at 460 nm) versus varying concentrations of AA

Table 1 Comparison of different methods for AA sensing

Materials	Methods	Linear range (μM)	LOD (μM)	Ref
PDA	Fluorescence	20–500	4.8	[32]
Eu-SiMoW	Luminescence	100–900	4.67	[33]
GSH-AuNCs	Fluorescence	350–700	200	[34]
LaF_3:Ce, Tb NPs	Fluorescence	8 – 100	2.4	[35]
TiO_2/rGO	Colorimetric	25–725	1.19	[5]
GQD	Fluorescence	1–30	0.27	[28]
g-C_3N_4−CoOOH	Fluorescence	5–50	1.6	This work

PDA polydopamine, *GSH* glutathione, *rGO* reduced graphene oxide, *GQD* graphene quantum dots

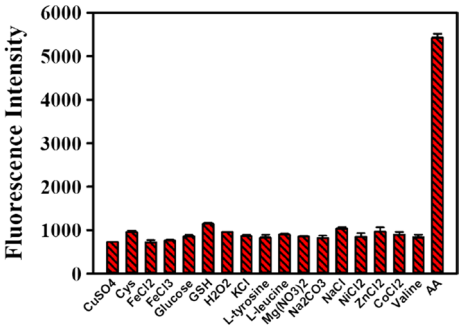

Fig. 4 Selectivity of the g-C_3N_4–CoOOH nanocomposite for AA (50 μM) over other species (500 μM)

Imaging of AA in living cells

We further explored the application of the g-C_3N_4–CoOOH nanocomposites to image AA in live cells. First, we examined the stability of the g-C_3N_4–CoOOH nanocomposites in live cells. As shown in Fig. S6, the results showed the g-C_3N_4–CoOOH nanocomposites were stable in live cells, due to the fact that the g-C_3N_4–CoOOH nanocomposites in the RPMI 1640 medium exhibited no sediment, even if 100 μg·mL^{-1} g-C_3N_4–CoOOH nanocomposites in the RPMI 1640 medium incubated for 7.5 h. And we also compared the fluorescence of the 100 μg·mL^{-1} g-C_3N_4–CoOOH nanocomposites in Tris buffer and RPMI 1640 medium for 2.5 h. The results showed no obvious fluorescence change. Then, we investigated the cytotoxicity of the nanocomposite by using the MTS assay. As shown in Fig. S7, the HeLa cells were incubated with different concentration of the nanocomposites (0, 50, 100, 150, 200, and 250 μg·mL^{-1}, respectively) for 2.5 h, 5.0 h and 7.5 h, respectively. The cell viability was above 80% even at the concentration of the nanocomposites up to 250 μg·mL^{-1} for 7.5 h. The results indicated that the nanocomposites exhibited very low cytotoxicity and good biocompatibility in live cells.

Then, we performed the imaging of AA in living cells. After incubation with the nanocomposite in the RPMI-1640 medium at 37 °C for 2.5 h, the L02 cells presented negligible fluorescence signal, revealing that a small amount of AA was in normal cells (Fig. 5A,a). The HeLa cells showed a slight fluorescence signal (Fig. 5A,b), which might be produced by the endogenous AA in live cells. To further confirm the assumption, we pretreated the HeLa cells with 10 U·μL^{-1} ascorbate oxidase (AOase), which was an inhibitor of the endogenous AA in live cells. The HeLa cells treated with the AOase showed an extremely weak fluorescence, indicating the slight fluorescence signal in cells without the treatment of the AOase was produced by the endogenous AA, revealing that the endogenous AA could trigger the fluorescence enhancement in live cells (Fig. 5A,c). To further validate that g-C_3N_4–CoOOH nanocomposites could react with AA concentration, we treated the HeLa cells with g-C_3N_4–CoOOH nanocomposites (100 μg·mL^{-1}) for 2.5 h, and then incubated with a different concentration of AA (50 μM, 100 μM) for another 2 h. As shown in Fig. 5A,d, there is significantly increased fluorescence with the treatment of 50 μM AA. And

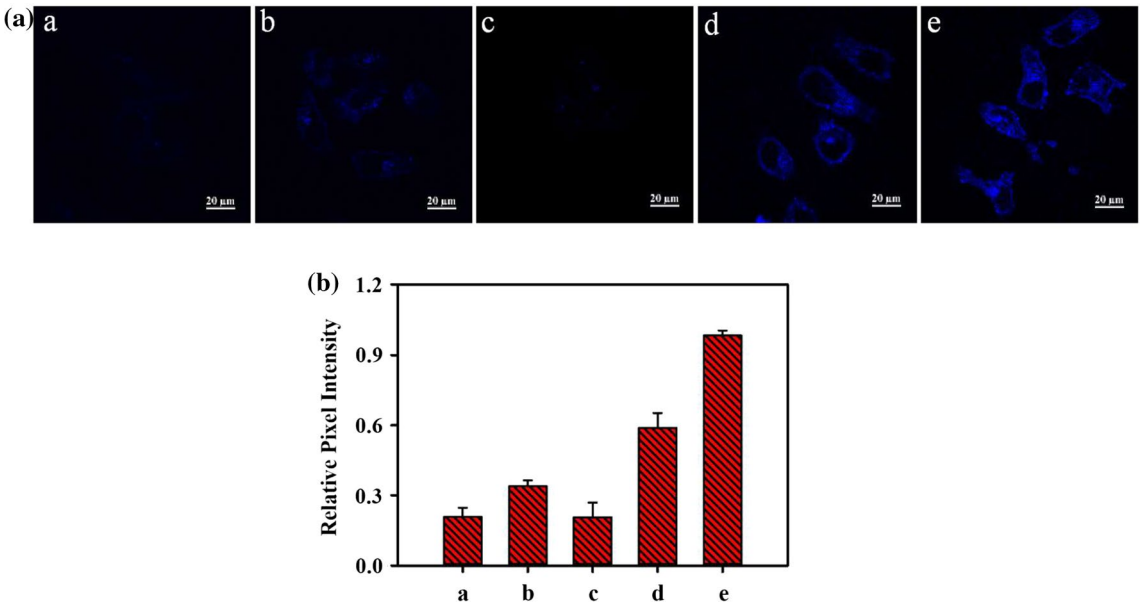

Fig. 5 Fluorescence images **A** and average fluorescence intensity **B** of (a) the L02 cells treated with g-C_3N_4–CoOOH nanocomposites (100 μg·mL^{-1}) only, the HeLa cells treated with (b) g-C_3N_4–CoOOH nanocomposites (100 μg·mL^{-1}) only, (c) AOase and g-C_3N_4–CoOOH nanocomposites (100 μg·mL^{-1}), (d) g-C_3N_4 – CoOOH nanocomposites (100 μg·mL^{-1}) and 50 μM AA, (e) g-C_3N_4 – CoOOH nanocomposites (100 μg·mL^{-1}) and 100 μM AA

HeLa cells treated with 100 μM AA showed brighter fluorescence than the HeLa cells treated with 50 μM AA (Fig. 5A,e). Therefore, these results implied that the nanocomposites could monitor the changes of the intracellular AA in live cells. Simultaneously, we used Olympus software to analyze the quantized mean blue intensity of HeLa cells (Fig. 5B). The results showed the fluorescence intensity was increased with the increase of AA concentration. It indicated this nanocomposite could image AA in live cells.

Conclusions

In summary, we developed a novel fluorescent nanoprobe (g-C_3N_4−CoOOH nanocomposites) that provided a rapid, and sensitive method to detect and image AA in live cells. As an emerging carbon-based nanomaterial, g-C_3N_4 nanosheets take the advantage of high fluorescence quantum yield and surface-to-volume ratio. In this system, the CoOOH nanosheets as a common quencher were in situ deposited on the surface of the g-C_3N_4 and efficient energy transfer-based fluorescence quenching of the g-C_3N_4. However, when the AA were added into the reaction system, the AA could reduce CoOOH to Co^{2+}, resulting in the fluorescence recovery of the g-C_3N_4−CoOOH nanocomposites. Furthermore, taking the advantage of low cytotoxicity, easy preparation, and low cost, we confirmed that the g-C_3N_4−CoOOH nanocomposites could successfully be applied to image the changes of the AA in live cells. We believe that our study holds great potential for broadening application of the nanomaterial based on g-C_3N_4 in bioimaging.

Supplementary Information The online version contains supplementary material available at https://doi.org/10.1007/s44211-022-00178-4.

Author contributions C.L.: investigation and writing—original draft. X.L.: conceptualization. L.D.: writing—review and editing and data curation. T.W.: formal analysis. H.Y.: methodology and supervision. G.Z.: methodology and supervision.

Funding Financial support was from the Scientific Research Fund of Hunan Provincial Education Department (21C0566) and Hunan Provincial Innovation Training Program for College Students (202211342042).

Declarations

Conflict of interest The authors declare that they have no known competing financial interests or personal relationships that could have appeared to influence the work reported in this paper.

References

1. R.R. Becker, H.B. Burch, L.L. Salomon, T.A. Venkitasubramanian, C.G. King, J. Am. Chem. Soc. **1953**, 75 (2020)
2. M.B. Ann, Adv. Pharmacol. **38**, 21 (1996)
3. A.C. Carr, B. Frei, Am. J. Clin. Nutr. **69**, 1086 (1999)
4. S.J. Padayatty, H.D. Riordan, S.M. Hewitt, A. Katz, L.J. Hoffer, M. Levine, CMAJ **174**, 937 (2006)
5. F.A. Harraz, M. Faisal, A.A. Ismail, S.A. Al-Sayari, A.E. Al-Salami, Al-Hajry, J. Electroanal. Chem. **832**, 225 (2019)
6. X.Q. Wu, J.G. Ma, H. Li, D.M. Chen, W. Gu, G.M. Yang, P. Cheng, Chem. Commun. **51**, 9161 (2015)
7. P.X. Huang, W.J. Kong, S. Wang, R.L. Wang, J.H. Lu, M.H. Yang, J. Pharm. Pharmacol. **70**, 1378 (2018)
8. N. Li, Y. Li, Y. Han, W. Pan, T. Zhang, B. Tang, Anal. Chem. **86**, 3924 (2014)
9. L. Li, C. Wang, K. Liu, Y. Wang, K. Liu, Y. Lin, Anal. Chem. **87**, 3404 (2015)
10. E. Lozinsky, V. Martin, T. Berezina, A. Shames, A. Weis, G. Likhtenshtein, J. Biochem. Biophys. Method **38**, 29 (1999)
11. T. Yang, B. Zheng, H. Liang, Y. Wan, J. Du, D. Xiao, Talanta **132**, 191 (2015)
12. L.L. Feng, Y.X. Wu, D.L. Zhang, X.X. Hu, J. Zhang, P. Wang, Z.L. Song, X.B. Zhang, W.H. Tan, Anal. Chem. **89**, 4077 (2017)
13. C. Tan, X. Cao, X.J. Wu, Q. He, J. Yang, X. Zhang, J. Chen, W. Zhao, S. Han, G.H. Nam, Chem. Rev. **117**, 6225 (2017)
14. X. Zhang, X. Xie, H. Wang, J. Zhang, B. Pan, Y. Xie, J. Am. Chem. Soc. **135**, 18 (2013)
15. S.A. Kitte, F.A. Bushira, C. Xu, Y. Wang, H.J. Li, Y.D. Jin, Anal. Chem. **94**, 1406 (2022)
16. S.H. Cao, H. Chen, F. Jiang, Z.X. Hu, ACS Appl. Mater. Int. **10**, 44624 (2018)
17. A. Ahmed, P. John, M.H. Nawaz, A. Hayat, M. Nasir, ACS Appl. Nano Mater. **2**, 5156 (2019)
18. X. Liao, Q. Wang, H. Ju, Chem. Commun. **50**, 13604 (2014)
19. S.G. Liu, L. Han, N. Li, Y.Z. Fan, Y.Z. Yang, N.B. Li, H.Q. Luo, Sensor Actuat. B-Chem. **283**, 515 (2019)
20. X.L. Zhang, C. Zheng, S.S. Guo, J. Li, H.H. Yang, G. Chen, Anal. Chem. **86**, 3426 (2014)
21. J.W. Liu, Y.M. Wang, C.H. Zhang, L.Y. Duan, Z. Li, R.Q. Yu, J.H. Jiang, Anal. Chem. **90**, 4649 (2018)
22. H.J. Zhang, A.R. Ding, B.T. Ye, Z.Q. Wang, J.W. Zhang, L.P. Qiu, J.H. Chen, ACS Appl. Nano Mater. **4**, 8546 (2021)
23. M. Rong, L. Lin, X. Song, T. Zhao, Y. Zhong, J. Yan, Y. Wang, X. Chen, Anal. Chem. **87**, 1288 (2015)
24. B.Z. Zheng, J.Y. Fan, B. Chen, X. Qin, J. Wang, F. Wang, R.R. Deng, X.G. Liu, Chem. Rev. **122**, 5519 (2022)
25. R. Chen, J. Zhang, Y. Wang, X. Chen, J.A. Zapien, C.S. Lee, Nanoscale **7**, 17299 (2015)
26. H. Wan, Y. Zhang, W. Zhang, H. Zou, ACS Appl. Mater. Int. **7**, 9608 (2015)
27. F. Song, X. Hu, Nat. Commun. **5**, 1 (2014)
28. H.M. Meng, X.B. Zhang, C. Yang, H.L. Kuai, G.J. Mao, L. Gong, W.H. Zhang, S.L. Feng, J.B. Chang, Anal. Chem. **88**, 6057 (2016)
29. X. Bi, L. Luo, L. Li, X. Liu, B. Chen, T. You, Talanta **218**, 121159 (2020)
30. Z. Wu, D. Nan, H. Yang, S. Pan, H. Liu, X. Hu, Anal. Chim. Acta **1091**, 59 (2019)
31. J. Zhou, Y. Yang, C.Y. Zhang, Chem. Commun. **49**, 8605 (2013)
32. Y. Zhao, L. Li, R. Yu, T.T. Chen, X. Chu, Anal. Methods **9**, 5518 (2017)
33. Z. Fu, W. Gao, T. Yu, L. Bi, Talanta **195**, 463 (2019)
34. X. Yan, L. He, C. Zhou, Z. Qian, P. Hong, S. Sun, Chem. Phys. **522**, 211 (2019)
35. C. Mi, T. Wang, P. Zeng, S. Zhao, N. Wang, S. Xu, Anal. Methods **5**, 1463 (2013)